Advances in Sustainable Energies & Environment

Journal homepage: https://A-SEE.MazUST.ac.ir/

Research Article

CO Oxidation on CuO and Transition Metal Catalysts: Comparative Study of Varied Silica Structures within CeO_2-SiO_2 Mixed Oxides

Ali Samadian[a], Fereshteh Meshkani[a*], Sajad Mobini[a], Mehran Rezaei[b]

[a] *Chemical Engineering Department, Faculty of Engineering, University of Kashan, Kashan, Iran*
[b] *School of Chemical, Petroleum and Gas Engineering, Iran University of Science and Technology (IUST), Tehran, Iran*

ARTICLE INFO

Article history:
Received: 2025-02-19
Revised: 2025-03-07
Accepted: 2025-05-03
Published online: 2026-01-01

Keywords:
Cu-based catalysts;
Ceria-silica;
Oxide-supported catalysts;
CO oxidation.

ABSTRACT

The CeO_2-M (M: SiO_2, MCM-41, MCM-48, and SBA-15) powders were fabricated by various techniques and were used as support for the Cu-based catalysts in the CO oxidation process. TPR, XRD, and N_2 adsorption-desorption techniques were applied to characterize the specimens that were made. The prepared catalysts possessed high surface areas in a 121_572 m^2/g span. The catalytic outcomes revealed that the Cu catalyst supported on the CeO_2-SiO_2 displayed the highest performance. CO conversion increased rapidly to 65% at around 150 °C and slowly reached 100% at around 300 °C. The influence of the different active species (Cu, Co, Mn, and Fe) on the optimum support was investigated, and the findings indicated that the CO conversion was considerably higher over the Co catalyst. It was observed that the activity of the Co/CeO_2-SiO_2 specimen rose gradually to 100% at 200 °C. A microporous and mesoporous structure with a narrow pore size distribution was also confirmed. The pretreatment tests also showed an affirmative trace of oxidative pretreatment on the catalytic efficiency. The stability tryout of the CO oxidation over the Co/CeO_2-SiO_2 model under dry and wet feed status during 36 h displayed high durability without any drop in CO conversion.

GRAPHICAL ABSTRACT

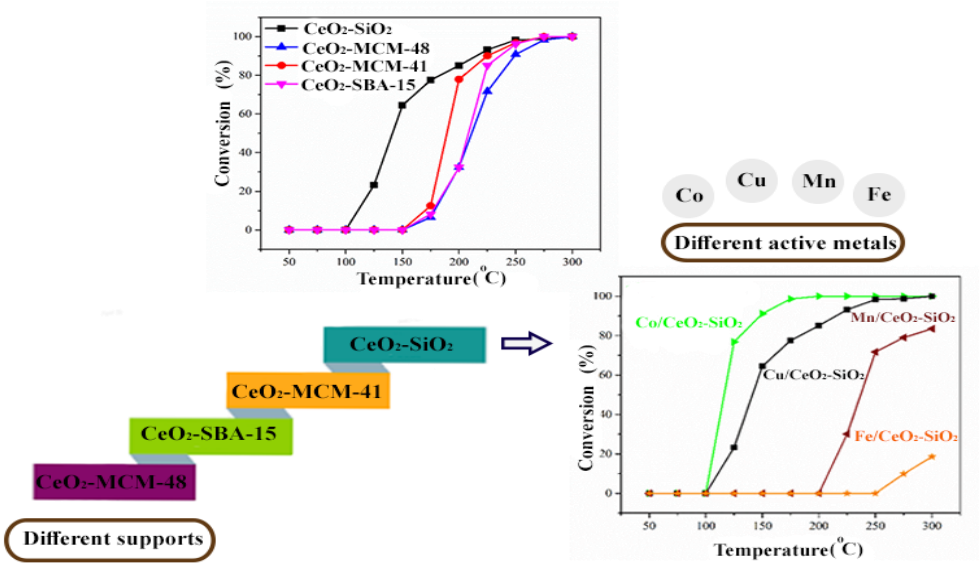

*** Corresponding author:**
E-mail address: *meshkani@kashanu.ac.ir*

Cite this article as:

Samadian, A., Meshkani, F., Mobini, S., & Rezaei, M. (2026). CO Oxidation on CuO and Transition Metal Catalysts: Comparative Study of Varied Silica Structures within CeO_2-SiO_2 Mixed Oxides. *Advances in Sustainable Energies & Environment.* https://doi.org/10.22034/a-see.2025.2053863.1001

1. Introduction

One of the major components of exhaust gas with easy distribution in the air and its pollution is carbon monoxide (CO), a colourless, odourless, and very toxic gas. The inhalation of carbon monoxide, even at the ppm level, harms human and animal life [1-3]. Oxygen can replace carbon monoxide, so it blends with hemoglobin and damages the focal nervous system. From the environmentalist's perspective, catalytic CO oxidation has been discussed as an impressive method of removing CO. In consequence, the survey of catalytic CO oxidation has imbibed much notice [3, 4]. In heterogeneous catalysis, one of the important goals is exploring the communication between the catalytic behaviour and the electronic structure of the active sites. Thereby, many kinds of research were carried out on optimizing and sketching new catalysts with high activity. The oxide-supported catalysts were widely used as important catalysts in the industry [5]. Generally, the supports used for CO oxidation are usually ceria, alumina, silica, zirconia, and titanium oxide [6, 7]. Metal-supported specimens on diverse oxides have distinct catalytic attributes related to the reducibility of the oxide, the surface acidity, thermal stability, special surface, and the metal-oxide interaction/reaction [8]. Amid the multiple carriers, the ceria–silica mesoporous functional composites are proper choices for various catalytic applications containing catalytic gas-phase oxidative dehydrogenation of propane [9], organic transformation in the liquid phase [10, 11], and specifically for CO oxidation [12, 13].

Ceria and ceria-based materials have excellent oxygen capacity [14, 15]. This feature helps the oxygen molecules to be adsorbed better on the catalyst's surface. Furthermore, mesoporous silica materials have special architecture and structural and unique properties such as thermal and mechanical stability and high surface area. Hence, the combination of these two supports can cause very unique properties. It is reported that ceria-silica composites with different compositions have high specific surface (S_{BET}) and thermal stability [12, 13], which can be considered as a suitable support for different metal nanoparticles [10].

Gonçalves et al. confirmed that the type of carrier has a potent effect on the catalytic performance. They presented that silica-supported catalyst shows higher activity than other supports for carbon monoxide oxidation in the following order: $CuO\text{-}CeO_2/SiO_2 > CuO\text{-}CeO_2/ZrO_2 > CuO\text{-}CeO_2/Al_2O_3$ [16]. Pal et al. reported that the Ce-MCM-41 and Ce-MCM-48 materials possessed highly ordered mesostructures. Also, silica-ceria composites showed a high surface area (349 m^2/g), significant activity, and good stability in oxidation processes [11]. The catalytic CO oxidation over Co_3O_4 catalysts has also been one of the hot spots in the field of heterogeneous catalysis. In fact, among the transition metal oxides, Co_3O_4 demonstrates the highest catalytic activity for the CO combustion and of organic compounds, and it could be included in formulations of catalysts for the treatment of waste gases [17-19]. Iron oxides and their composite oxides are also used as catalysts and support in CO oxidation [20-22]. Rida et al. prepared bimetallic Co-Fe and Co-Cr catalysts supported on CeO_2 for CO oxidation. They found that replacing Fe instead of Cr improved the catalytic activity. It is reported that introducing Fe to the catalyst increased the activity at low temperatures, which is attributed to the influence of the formed $CoFe_2O_4$ phase [23]. Ravandi and Rezaei investigated the CO oxidation over iron–cobalt mixed oxide nanocatalysts with different Co/Fe molar ratios [24]. Their catalytic outcomes indicated that adding cobalt to iron oxide, even in a small amount, has a visible effect on rising CO conversion at lower temperatures. Wu et al. designed $PtCo/Co_3O_4\text{-}SiO_2$ catalysts where the strong metal−support interactions between PtCo nanoalloys and $Co_3O_4\text{-}SiO_2$ supports can create lots of active lattice oxygen to improve the catalytic performance for CO oxidation in water vapour and render structural stability [25].

According to the above description, combining silica and cerium could be a promising candidate for catalyst support in CO oxidation reactions. Since no systematic survey has been done on the study of the composition of cerium and various silica structures as a support for the CO oxidation reaction, in this paper, we have tried to achieve the best structure of silica-cerium composite for this reaction. After that, different active metals were embedded in the optimum support, and the catalytic performance of the manufactured specimens was evaluated.

2. Experimental

2.1 Materials

All starting materials including cerium nitrate hexahydrate (Merck, 99%), copper nitrate trihydrate (Merck, 99%), cetyl trimethyl ammonium bromide, CTAB (Merck), tetraethyl orthosilicate, TEOS (Merck, >98%), ethanol (Scharlau,99.2% w/w), ammonium hydroxide (Merck, 25%), Pluronic P123 (Aldrich, Mw∼5800), cobalt nitrate trihydrate (Merck, 99%), manganese nitrate trihydrate (Merck, 99%) were used without any purification.

2.2 Preparation of CeO_2-M (SiO_2, SBA-15, MCM-48 and MCM-41) composites

The Ceria-SiO_2 composite powder was fabricated by a simple sol-gel procedure [26]. In summary, 6.057 g of EtOH, 0.665 g of NH_4OH, and 0.722 g of $Ce(NO_3)_3.6H_2O$ were dissolved in deionized water. Simultaneously, 3.467 g TEOS with 6.057 g of EtOH were dissolved in another beaker. Then, two solutions were mixed, and the final mixture was held under stirring for 24 h at ambient temperature. After that, the mixture was cooled to room temperature, and the suspension was dried to acquire solid powder for 12 h at 80°C in an oven, and the

powder was calcined at 500°C for 4 h. Ceria-SBA-15 composite powder was fabricated matching the procedure explained in the literature [27]. In a typical synthesis, P123 (2.557 g) as the structure-directing factor was dissolved in deionized water, and then 15.766 g of HCl (2M) solution was added to this solution under stirring. Afterward, 0.546 g of the TEOS was poured slowly into this acidic solution. Then, 0.227 g $Ce(NO_3)_3.6H_2O$ was entered into the above liquid mixture, and stirring was continued for 24 h at room temperature. The obtained suspension was moved to a Teflon-lined stainless-steel autoclave and heated at 100 °C for 24 h. The white product was washed, dried at 100 °C and calcined at 550 °C for 5 h for the complete elimination of the template.

The Ceria-MCM-48 sort mesoporous silica was made using the sol-gel method [11]. Firstly, 1.2 g of CTAB was dissolved in an admixture of 50 mL deionized water and 15 mL of EtOH. Then, 6 mL of NH_4OH was poured into the obtained solution under severe stirring. With 30 minutes passed, 1.8 mL of TEOS was put into the surfactant solution, and the mixture was stirred for one more 30 min until a hefty white precipitate was created gently. In another bottle, 0.35 g (0.81 mmol) of $Ce(NO_3)_3.6H_2O$ was dissolved in 10 mL of EtOH, and then this solution was added slowly to the prior mixture. The terminal mixture was held under stirring for 24 h at ambient temperature, pursued by aging for another 24 h without stirring at 100 °C. Afterward, the mixture was cooled to room temperature, filtered, and washed several times with deionized water. The material was dried and calcined at 550 °C for 5 h. Ceria-MCM-41 type mesoporous silica readied by a sol-gel procedure [28]. For a classic synthesis, 0.874 g CTAB was dissolved in 20.73 g distilled water. Then 21.37 g ethanol and 10.63 g ammonium hydroxide were added to this solution and stirred for 30 min. After that, 1.733 g TEOS was surcharged under stirring, and the obtained mixture was stirred for 15 min—eventually, 0.722 g $Ce(NO_3)_3.6H_2O$ was added to the mixture and then aged for 24 h under stirring, and after filtration, washing, and drying, the dried powder was calcined at 550 °C for 5h. In all synthesized compounds, the mass ratio of cerium/silica was maintained at 1 to 9.

2.3 Catalyst preparation

The catalysts with 10 wt.% active metal were prepared by impregnating the supports with a solution of metal nitrate precursors at the desired concentration. The impregnation was carried out at room temperature for 4 hours, after which the suspension was dried at 80°C and calcined at 500°C for 4 hours.

2.4 Characterization

The X-ray diffraction (XRD) analysis was fulfilled using an X-ray diffractometer (PANalytical X'Pert-Pro) with a Cu-K monochromatized radiation source and a Ni filter in the range 2θ=10-80°. The N_2 adsorption/desorption analysis (BET) was performed at -196 °C using an automated gas adsorption analyzer (Belsorp mini II). Temperature programmed reduction (TPR) analysis was carried out with Micromeritics chemisorb 2750 gas-adsorption equipment to investigate the reduction properties of the catalysts. In the TPR analysis, about 100 mg catalyst was exposed to a heat treatment (10°C/min) in a gas flow (30 ml/min) containing a mixture of H_2: Ar (10:90). Before the TPR experiment, the catalysts were pretreated under an Ar atmosphere at 200°C for 1 hour.

2.5 Catalytic evaluation

Carbon monoxide oxidation was accomplished under atmospheric pressure in a quartz tubular fixed bed flow reactor (ID 7mm x 500mm long). For each test, 100 mg of the readied material was sieved to 35-70 mesh and charged into the reactor. The reaction temperature was measured and controlled using an Omega K-type thermocouple placed under the catalyst bed. The feed gas composition contained 2% CO and 20% O_2 and was balanced with Ar at a gas hourly space velocity (GHSV) of 60,000 ml/g_{cat} h. Before the reaction, the samples were oxidized in situ by a mixture flow of O_2 (10 ml/min) and Ar (40 ml/min) at 300°C for 1 h. The performance examinations were investigated at several temperatures from 50 to 300°C in periods of 25°C, which was retained for 40 min at each temperature. A gas chromatograph (Varian, model 3400) equipped with a TCD detector fulfilled the scrutiny of the effluent gases from the reactor. According to Eq. 1, CO conversion was described as the number of moles of CO consumed after the reaction concerning the quantity of inlet CO in the feed gas CO.

$$\text{Conversion (\%)} = \frac{\text{COin} - \text{COout}}{\text{COin}} \quad (1)$$

Also, for more details, the rate of reaction was calculated from the following equation (Eq. 2):

$$\text{Rate of reaction} = \frac{\text{CO}_2\text{ produced (ccm)} \times (1\text{mol}/22400\text{cc})}{0.1 \times 60(\text{sec}/\text{min})} \quad (2)$$

Where, 0.1 is the amount of catalyst that is used in the process. All atoms of different active phases (Cu, Co, Mn, and Fe) were assumed to be on the surface, hence from the known weight of the catalyst and the metals loading. TOF was calculated from the following equation (Eq. 3):

$$\text{TOF} = \frac{\text{CO}_2\text{ produced (mol/s)}}{\text{m}} \quad (3)$$

Where, *m* is the weight of different active phases in the catalyst.

3. Results and discussion

3.1 Evaluation of different supports

The XRD patterns of the CuO-based catalysts supported on various CeO_2-M (m: SiO_2, SBA-15, MCM-48, and MCM-41) composites are shown in Fig. 1. For the Cu/CeO_2-SiO_2 and Cu/CeO_2-MCM-41 catalysts, the peaks at 2θ=28.76°, 33.23°, 47.69°, 56.52° and 76.9° are related to the cerium oxide (JCPDS. 00-001-0800) [29], and the diffraction peaks at 2θ= 28.76° and 33.23° are related to the silicon oxide (JCPDS. 00-047-1300) [30]. The intensity of these peaks decreased for the

Cu/CeO_2-MCM-41 catalyst and completely disappeared for the Cu/CeO_2-MCM-48 and Cu/CeO_2-SBA-15 samples. The decrease in the peak intensity confirmed the higher dispersion of ceria particles in the silica structure for these samples. Also, these results indicated the high specific surface area and amorphous structure of MCM-48 and SBA-15 types mesoporous silica [9]. The characteristic XRD patterns of CuO were also observed for all samples at 2θ = 35.7° and 38.89° (JCPDS. 01-089-2531), which reveals the formation of crystalline metal oxide particles [31].

Scherrer's equation computed the crystallite sizes of copper and cerium oxides according to the diffraction peaks located at 2θ=35.70° and 2θ=33.23°, respectively, and the results are summarized in Table 1.

As can be seen, the Cu/ CeO_2-SiO_2 catalyst possessed the smallest CuO crystal size compared to other prepared catalysts.

The textural features of the CuO catalysts supported on several carriers are reported in Table 1. The lowest and the highest BET surface area and corresponding pore volume were observed for Cu/CeO_2-SiO_2 and Cu/CeO_2-SBA-15 catalysts, respectively. Also, the theoretical particle sizes were computed from the formula (4):

$$D_{BET} = \left(\frac{6000}{\rho \times s}\right) \quad (4)$$

Where D_{BET} is the equivalent particle diameter in nanometers, ρ is the density of the material in g/cm^3, and S is the specific surface area in m^2/g. It is obvious from Table 1 that the particles with the higher surface area have smaller particle sizes. For example, the smallest particle scale is related to the Cu/CeO_2-SBA-15 specimen with a great surface area.

Also, the N_2 adsorption-desorption isotherms and the corresponding BJH pore size distribution curves of the CuO-supported catalysts are indicated in Fig. 2a and 2b, respectively. Except for the Cu/CeO_2-SBA-15 sample, the rest of the samples displayed a type II isotherm with an H3-type hysteresis loop, whereas the Cu/CeO_2-SBA-15 sample presented a type IV isotherm with an H1-type hysteresis loop. Type II isotherms are associated with materials with non-porous, macroporous, and uniform surfaces, such as silica, which have multilayer adsorption. The Type IV isotherm is related to materials with mesoporous structures, such as amorphous silica (SBA-15) [32, 33].

In this type of adsorption isotherm, both the adsorption volume and rate rise with relative pressure, and the first half of the isotherm is similar to the type II isotherm [34]. The H1-type hysteresis loop is related to the porous substances, expressing a narrow distribution of relatively uniform (cylindrical-like) pores, and the H3-type hysteresis loop does not depict any limiting adsorption at high P/P_0 [34-36]. In the Cu/CeO_2-SBA-15 catalyst case, the hysteresis loop is observed in the relative pressure (p/p_0) range of 0.4–0.9, indicating the presence of small mesopores. The quick enhancement in the amount of adsorbed volume of N_2 in low relative pressure (lower than 0.2) confirmed the presence of some micropores in its structure.

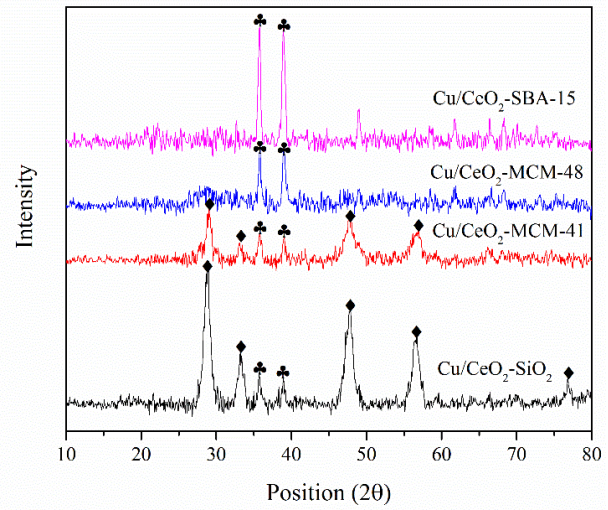

Fig.1. XRD patterns of CuO-based catalysts supported on several CeO_2-M (M: SiO_2, SBA-15, MCM-48, and MCM-41) composites (♦ CeO_2, ♥ SiO_2, ♣ CuO)

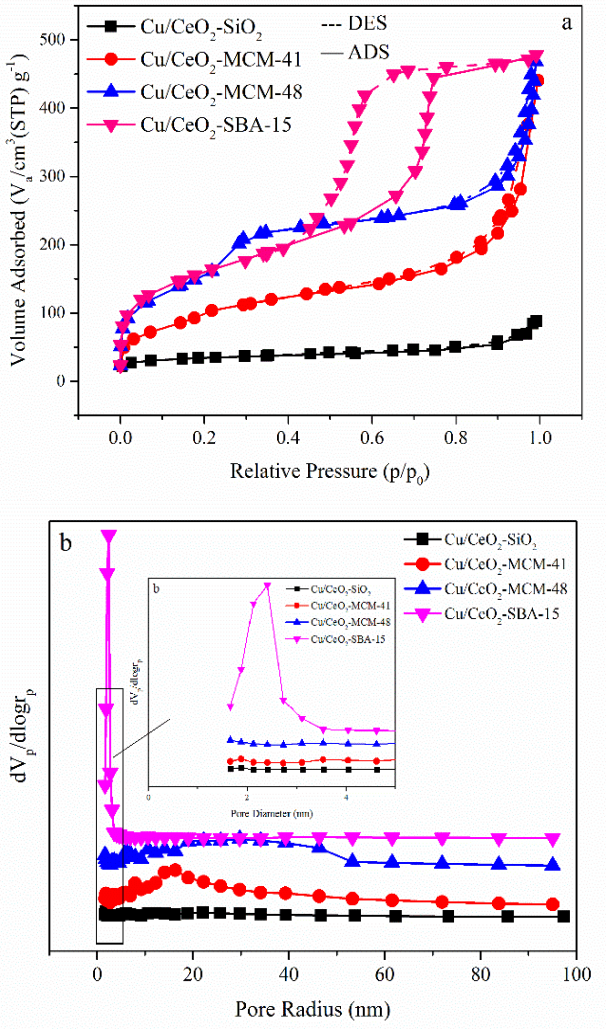

Fig.2. (a) N_2 adsorption/desorption isotherms and (b) pore-size distributions of the CuO catalysts supported on various CeO_2-M (m: SiO_2, SBA-15, MCM-48, and MCM-41) composites

Table 1. Textural attributes of the CuO- supported on numerous CeO_2-M (M: SiO_2, SBA-15, MCM-48, and MCM-41) composites

Sample	Surface area ($m^2\ g^{-1}$)	Mesopore volume ($cm^3 g^{-1}$)	Mesopore size (nm)	$D_{particle}$ (from BET data) (nm)	$D_{crystal}$ (from Scherrer equation) (nm)	
					CuO	CeO_2
Cu/ CeO_2-SiO_2	121.7	0.13	4.37	12.85	15.9	10.5
Cu/ CeO_2-MCM-41	359.2	0.52	5.82	4.26	20.6	8.7
Cu/ CeO_2-MCM-48	570.9	0.57	4.05	2.68	27.4	-
Cu/ CeO_2-SBA-15	572.4	0.59	4.16	2.67	19.8	-

For the Cu/CeO_2-MCM-41 catalyst, a hysteresis loop in the relative pressure span of 0.5-1.0 represents its mesoporous structure. Creating a hysteresis ring at the higher relative pressures in Cu/CeO_2-MCM-48 and Cu/CeO_2-SiO_2 catalysts indicates the presence of larger pores in these catalysts. From pore size distribution curves of the samples (Fig. 2b), the Cu/CeO_2-SiO_2, Cu/CeO_2-MCM-48, and Cu/CeO_2-MCM-41 catalysts represented no distribution of pores in the meso zone. Meanwhile, the Cu/CeO_2-SBA-15 catalyst revealed a narrow pore size distribution in meso-areas (1-4 nm).

The H_2-TPR bends of the models are shown in Fig. 3. The reduction curves of all samples are characterized by a sharp peak at about 250 °C. According to previous studies [37], this case can be related to one kind of CuO species in the structure and the reduction of Cu^{2+} to Cu^0. This case showed that the CuO particles are well dispersed on the supports. This peak shifts to a higher temperature of around 300 °C for the Cu/CeO_2-MCM-48 sample. The Cu/CeO_2-MCM-48 also indicated a small peak at about 210 °C, which could be related to reducing the CuO clusters with weak interaction with CeO_2 [38]. Also, the formation of the other reduction peak at higher temperatures (~700 °C) in Cu/CeO_2-MCM-41 can be due to the interactions of CuO particles with supports. Regarding the peak area, it is observed that the recovery rates of the Cu/CeO_2-SiO_2 and Cu/CeO_2-MCM-41 catalysts are more reducible, with a small, broad peak at 858 °C, which can be attributed to the reduction of ceria [39].

The catalytic conversion of CO over the CuO-supported with several CeO_2-M composites is shown in Fig. 4. It is obvious from the figure that for all catalysts, CO conversion increased with the reaction temperature, and CeO_2-SiO_2 showed the best performance as a support for CuO in CO oxidation which may be owing to the high crystallinity of this catalyst as presented in the XRD analysis. A rising trend in the Cu/CeO_2-SiO_2 model activity was observed, followed by an increase in temperature so that the CO conversion grew swiftly up to 65% at around 150 °C and then slowly reached 100% at around 300 °C. For the Cu/CeO_2-MCM-41, Cu/CeO_2-MCM-48, and Cu/CeO_2-SBA-15 catalysts, CO conversion started from 150 °C and achieved 100% conversion at 275 °C for Cu/CeO_2-MCM-41 and Cu/CeO_2-SBA-15 and 300 °C for Cu/CeO_2-MCM-41. The CuO/CeO_2-MCM-41 sample showed higher catalytic activity than CuO/CeO_2-MCM-48 and CuO/CeO_2-SBA-15 catalysts. The cause for the lower performance of the two catalysts can be related to the lack of the formation of the ceria crystalline phase in the prepared catalysts. A superb choice for oxidation reaction is CeO_2, which usually does not require pretreatment because of its great oxygen exchange capability. It aids in boosting the adsorption/desorption of oxygen species on the metal bed and simplifies the reaction with adsorbed carbon monoxide [3].

For the catalytic performance of the catalysts, $T_{50\%}$ and $T_{100\%}$ were evaluated, and the consequences are briefed in Table 2. $T_{50\%}$ and $T_{100\%}$ are temperatures at which CO conversion reached 50% and 100%, respectively. Also, the turnover frequencies (TOF_{CuO}) and the reaction rates (µmol/g.s) were considered, relying on the activity findings and the moles of CuO in the various supported specimens. The TOF_{CuO} of the catalysts was calculated under GHSV = 60000 ml/g_{cat} h, CO/O2 = 2/20 molar ratio and a reaction temperature of 175 and 250 °C, Table 2.

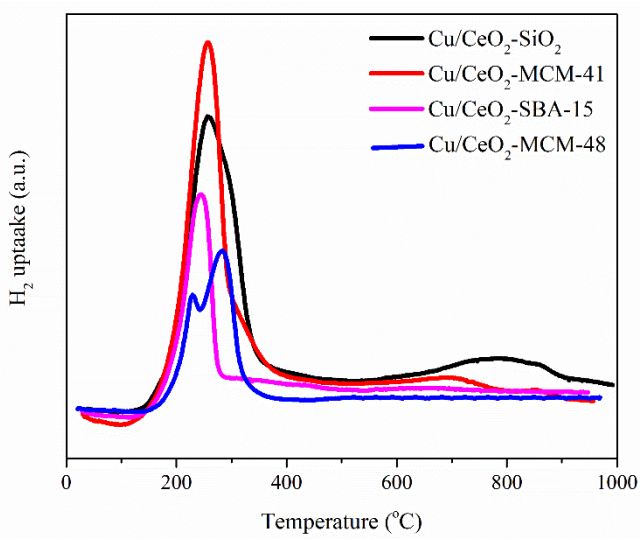

Fig.3. H_2-TPR profiles of CuO catalysts supported on various CeO_2-M (M: SiO_2, SBA-15, MCM-48 and MCM-41) composites

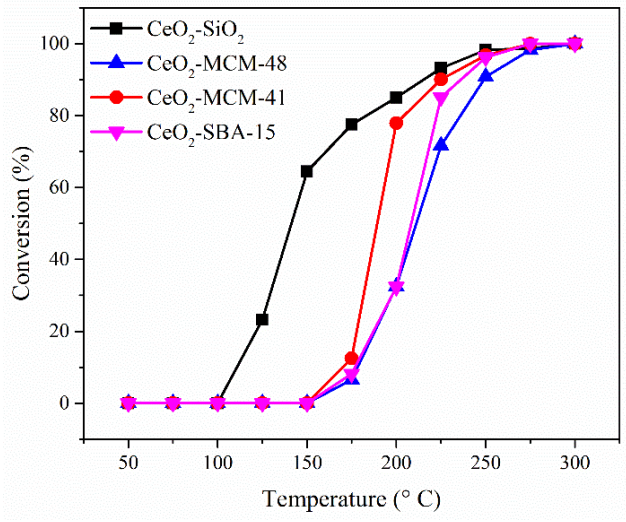

Fig.4. CO conversion over the CuO catalysts supported on various CeO_2-M (m: SiO_2, SBA-15, MCM-48 and MCM-41) composites. ($[CO]_{in}$=2 ml/min, $[O_2]_{in}$ = 20 ml/min and $[Ar]_{in}$ = 78 ml/min, GHSV = 60000 ml/g_{cat} h)

Table 2. Catalytic activity, reaction rate, and TOF_{Cu} values at 175 and 250 °C for the CO oxidation reaction

Sample	CO oxidation at 175 °C		CO oxidation at 250 °C		CO oxidation activity	
	Reaction rate (μmol/g.s)	TOF ($\times10^{-5}$ s^{-1})	Reaction rate (μmol/g.s)	TOF ($\times10^{-5}$ s^{-1})	$T_{50\%}$(°C)	$T_{100\%}$(°C)
Cu/CeO_2-SiO_2	11.5	9.96	14.6	12.20	140	300
Cu/CeO_2-MCM-41	1.9	1.60	14.3	12.00	180	225
Cu/CeO_2-MCM-48	1.2	1.04	13.5	11.80	205	300
Cu/CeO_2-SBA-15	1.2	1.14	14.4	11.92	210	275

As can be seen, the TOF_{CuO} reached the highest value over the Cu/CeO_2-SiO_2 catalyst in the CO oxidation at 175 and 250 °C. Also, the Cu/CeO_2-SiO_2 catalyst showed the highest CO reaction rate at 175 and 250 °C.

3.2 *Evaluation of the various active metals supported on CeO_2-SiO_2*

According to the results obtained in the previous section, the CeO_2-SiO_2 support was chosen as the best support for evaluating the catalytic performance of other active components. For this purpose, various active components, including Fe, Mn, Co, and Cu, were impregnated on the CeO_2-SiO_2 support, and the structural characteristics and their catalytic performance were evaluated.

The XRD patterns of the catalyst with diverse active phases supported on CeO_2-SiO_2 are shown in Fig. 5. As shown in the figure, the formation of active metal oxide is detected in all samples. From the pattern of the Mn/CeO_2-SiO_2 sample, the peaks observed at 2θ = 28.76° and 56.52° (JCPDS. 00-050-0866) [40] are related to the MnO_x phase, and the peaks at 2θ=35.7° and 38.89° are attributed to the characteristic XRD patterns of CuO (JCPDS. 01-089-2531) in the Cu/CeO_2-SiO_2 sample. Also, the diffraction peaks at 2θ = 35.89°, 39.11°, and 56.52° can be assigned to the Co_3O_4 phase (JCPDS. 00-042-1300) [41], and the diffraction peaks at 2θ = 33.23° and 56.52° are related to Fe_2O_3 phase (JCPDS. 01-084-0308) [8, 26, 40] in Co/CeO_2-SiO_2 and Fe/CeO_2-SiO_2 samples, respectively. Furthermore, in all samples, cerium and silica crystalline phases are observed. Regarding the Co/CeO_2-SiO_2, the weak intensity summits indicated this catalyst's low crystallinity and small particle size.

Fig. 6a shows the N_2 adsorption-desorption isotherms of different catalysts. As seen, all specimens manifested a type II isotherm with an H3-type hysteresis ring. Generally, type II isotherms belong to the macroporous materials. According to this isotherm, it can be said that the particles have slit-shaped pores with non-uniform sizes [42-44]. At low pressures, the slope of the isotherms for Co/CeO_2-SiO_2 and Fe/CeO_2-SiO_2 catalysts is higher than that of the other catalysts. This shows that the level of single-layer nitrogen adsorption in these samples is higher, which indicates their higher surface area.

These results are confirmed in Table 3. Also, the formation of the hysteresis loop at the relative pressure of 0.4–1.0 in Co/CeO_2-SiO_2 and Fe/CeO_2-SiO_2 catalysts suggests the existence of the mesoporous structure. Plus, the BJH pore size distribution of the different models is demonstrated in Fig. 6b. Except for the Mn/CeO_2-SiO_2 sample, which revealed no distribution of pores in any area, other samples proclaimed a pore-extent distribution in micro and meso-areas.

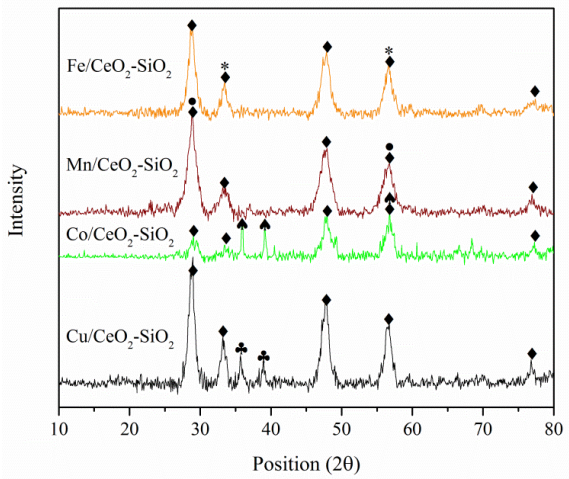

Fig.5. XRD patterns of the specimens with several active phases supported on CeO_2-SiO_2 (♦ CeO_2, ♥ SiO_2, ♣ CuO, ● MnO_2, ♠ Co_3O_4, * Fe_2O_3)

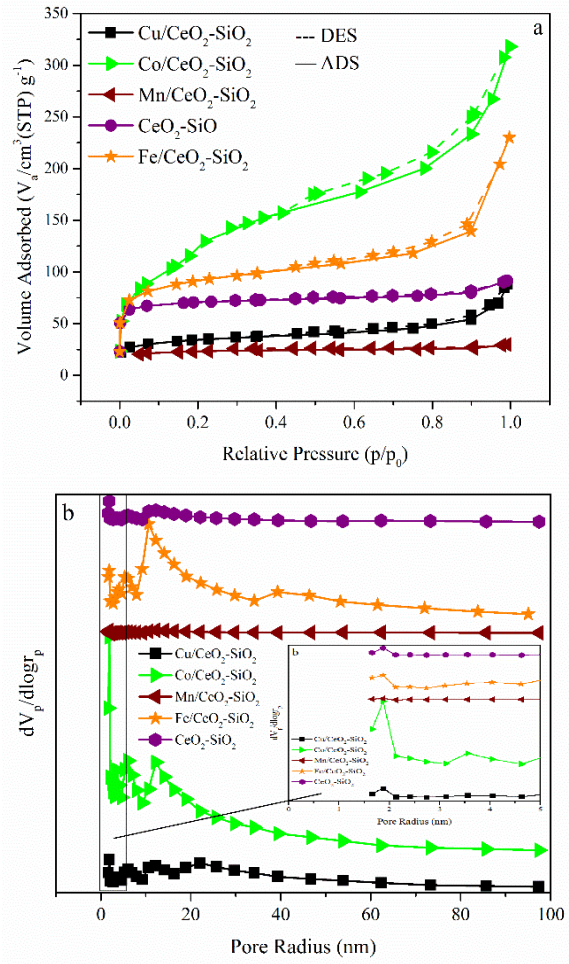

Fig.6. (a) N_2 adsorption/desorption isotherms and (b) pore-size distributions of the different catalysts with various active phases supported on CeO_2-SiO_2

The H_2-TPR profiles of the different prepared specimens have appeared in Fig. 7. The H_2-TPR profiles of CeO_2-SiO_2 support show two reduction peaks between 500 °C and 900 °C. According to the previous work [30, 45], it can be said that the initial summit at ~550 °C belongs to the reduction of surface adsorbed oxygen atoms from CeO_2 at low temperatures, and the second peak at around 850 °C is attributed to the reduction of bulk oxygen at higher temperatures.

The H_2-TPR profiles of the Co/CeO_2-SiO_2 catalyst include two principal reduction peaks at 210 °C and 280 °C, which are related to the two major stages of the reduction process, including Co_3O_4 to CoO and CoO to Co^0, respectively [45]. Another possibility is that these TPR peaks are related to the reduction of crystalline and dispersed CoO species [41]. According to the previous work [40, 46], it can be said that the prime peak at around 400 °C is identified as the reduction of MnO_2 or Mn_2O_3 to Mn_3O_4. Two other peaks at about 700 °C and 840 °C can be attributed to the reduction of ceria, which was shifted to the higher temperatures. Also, according to this figure, there are three peaks for Fe/CeO_2-SiO_2; the first peak (at around 420 °C) can be related to the reduction of Fe_2O_3 to Fe_3O_4. The second peak is broader and, at high temperatures, represents the reduction of Fe_2O_3 to Fe [40]. One other peak can be ascribed to the reduction of ceria. The Co/CeO_2-SiO_2 and Cu/CeO_2-SiO_2 samples have the highest degree of reducibility compared to other samples, which has a superior effect on their catalytic performance [37].

Fig. 8 shows the CO catalytic conversions over the different CeO_2-SiO_2 supported catalysts. The Co/CeO_2-SiO_2 specimen shows the supreme performance for CO oxidation compared to the other samples (Fig. 8). The high S_{BET} and pore volume of this sample are very important factors in its high activity. Furthermore, creating the Co_3O_4 spinel species helps improve this sample's performance. Co_3O_4 spinel oxide is identified as a very active species for the oxidation of carbon monoxide. This catalyst has Co^{3+} on octahedral coordination sites and Co^{2+} on tetrahedral coordination sites. Co^{3+} on the catalyst bed is commonly thought to provide the active areas for CO oxidation [47]. The formation of this phase has been proved by XRD and TPR analysis. It was observed that the activity of Co/CeO_2-SiO_2 was significantly enhanced with increasing temperature, reaching rapidly to nearly 80% at around 125 °C and then increasing gradually to 100% at around 200 °C. In the Mn/CeO_2-SiO_2 and Fe/CeO_2-SiO_2 catalysts, the catalytic activity is lower due to the low reducibility of these catalysts (Fig. 7). For Mn/CeO_2-SiO_2 catalyst, 50% CO conversion (T_{50}) was achieved at around 230 °C and did not complete below 300 °C. To better compare the catalytic performance, the CO oxidation rate, TOF number, $T_{50\%}$ and $T_{100\%}$ values are calculated and presented in Table 4. Xi et al. studied the promotional effects of CeO_2, MnO_2, and Fe_2O_3 on CuO/SiO_2 in CO oxidation reaction. Their CO oxidation test indicated that the CuO/CeO_2-SiO_2 has complete conversion of CO at 433 K and GHSV of 9000 ml/g_{cat} h [48]. Using chemical vapour deposition, Kouotou et al. fabricated cobalt-iron mixed oxide thin films with varying Co: Fe ratios. The complete CO oxidation for $Co_{0.9}Fe_{2.1}O_4$, $Co_{1.8}Fe_{1.2}O_4$, and $Co_{2.1}Fe_{0.9}O_4$ occurred at temperatures of 255°C, 275°C, and 325°C, respectively, under a GHSV of 45000 ml/g_{cat} h [49].

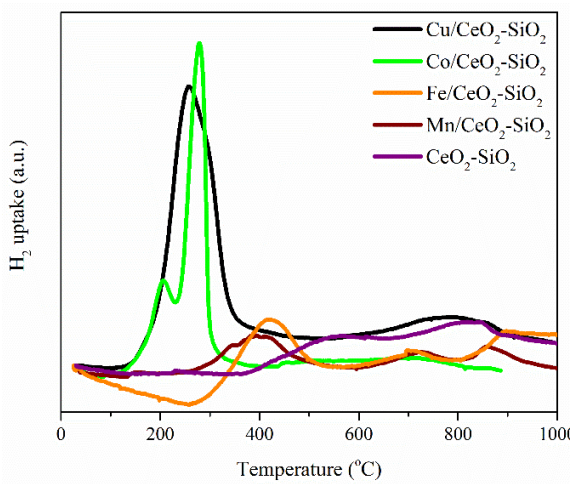

Fig.7. H_2-TPR profiles of the different catalysts with various active phases supported on CeO_2-SiO_2

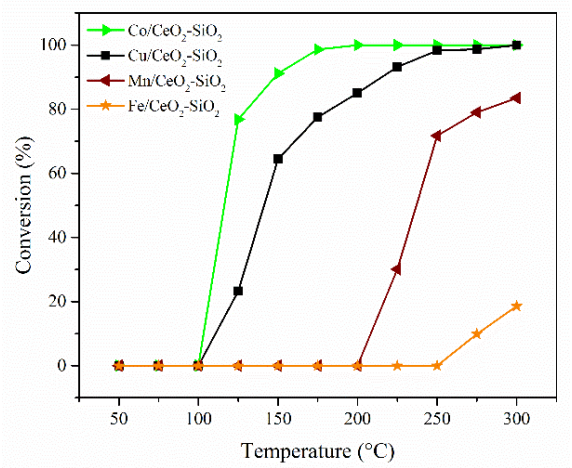

Fig.8. CO conversion over the different catalysts with various active phases supported on CeO_2-SiO_2. ($[CO]_{in}$ = 2 ml/min, $[O_2]_{in}$ = 20 ml/min and $[Ar]_{in}$ = 78 ml/min, GHSV = 60000 ml/g_{cat} h)

Table 3. Textural attributes of the catalysts with varied active phases supported on CeO_2-SiO_2

Sample	Surface area (m^2 g^{-1})	Mesopore volume (cm^3g^{-1})	Mesopore size (nm)	$D_{particle}$ (from BET data) (nm)	$D_{crystal}$ (from Scherrer equation) (nm)	
					MO_x	CeO_2
Cu/CeO_2-SiO_2	121.7	0.13	4.37	12.85	15.9	10.5
Co/CeO_2-SiO_2	403.7	0.47	4.72	3.86	38.5	24.1
Mn/CeO_2-SiO_2	90.2	0.04	2.04	13.22	21.9	8.3
Fe/CeO_2-SiO_2	324.3	0.27	3.44	4.85	13.6	11.6
CeO_2-SiO_2	272.8	0.14	2.07	6.86	-	-

M: different active phases (Cu, Co, Mn, and Fe)

Table 4. Catalytic activity, reaction rate, and TOF_M amounts at 175 and 250 °C for the CO oxidation reaction

Sample	CO oxidation at 175 °C		CO oxidation at 250 °C		CO oxidation activity	
	Reaction rate (μmol/g.s)	TOF ($\times10^{-5}$ s^{-1})	Reaction rate (μmol/g.s)	TOF ($\times10^{-5}$ s^{-1})	$T_{50\%}$ (°C)	$T_{100\%}$ (°C)
Cu/ CeO_2-SiO_2	11.5	9.96	14.6	12.20	140	300
Co/ CeO_2- SiO_2	14.7	1.72	14.9	1.75	110	200
Mn/ CeO_2- SiO_2	0.0	0.00	11	6.66	235	-
Fe/ CeO_2- SiO_2	0.0	0.00	1.5	0.00	~ 350	-
CeO_2- SiO_2	0.0	0.00	0.0	0.00	-	-

M=different active phase (Cu, Co, Mn, and Fe)

3.3 Evaluation of the influence of process parameters and stability on the catalytic activity

The effect of pretreatment on CO conversion of the Co/CeO_2-SiO_2 catalyst was investigated by conducting various pretreatment processes (oxidative, inert, and reductive atmospheres. Fig. 9 indicates the role of various pretreatment states on the performance of the Co/CeO_2-SiO_2 catalyst. In the case of pretreatment with an oxidative atmosphere, before the reaction, a gas stream with 20% O_2/Ar was entered into the catalyst bed at 300 °C for 1 h. Pure N_2 and 20% H_2/Ar were applied for inert and reductive atmospheres, respectively.

The outcomes showed that the oxidative atmosphere (O_2-pretreatment) had positive roles on the catalytic performance and improved the activity of the Co/CeO_2-SiO_2, which could be owing to the adsorption of oxygen on the catalyst's bed and hence facilitated access to the reactants to the active surface oxygen. On the other hand, the activity of the catalyst was reduced by using a reductive atmosphere (H_2-pretreatment), and using the inert atmosphere (N_2-pretreatment) had a moderate influence. Also, the important role of surface oxygen in the performance is understandable based on the results [46].

Fig. 10 illustrates the importance of gas hourly space velocity and feed ratio on carbon monoxide conversion over the Co/CeO_2-SiO_2 model. The CO conversion increased with a CO/O_2 molar ratio drop. Excess oxygen in the reactants ensures the replacement of superficial oxygen and subsequently improves the catalyst performance. Also, by enhancing the GHSV from 30,000 to 90,000 ml/g_{cat} h (Fig. 10b), CO conversion is reduced at a constant reaction temperature (150 °C). It can be due to the decrease in the contact time between the gas stream and the specimen bed that caused a decline in the activity [43].

The role of dry and wet feed states in checking the lifetime of the Co/CeO_2-SiO_2 model during 36 h was accomplished and presented in Fig. 11. A stable CO conversion is achieved in dry feed situations without any drop (2% CO and 20% O_2). Water vapour and CO_2 in the reactant substantially influence durability at the first 500 min, which causes a significant drop in initial conversion. This is because moisture is adsorbed onto active sites by water, and the metal oxide surface is covered by CO_2 molecules [46].

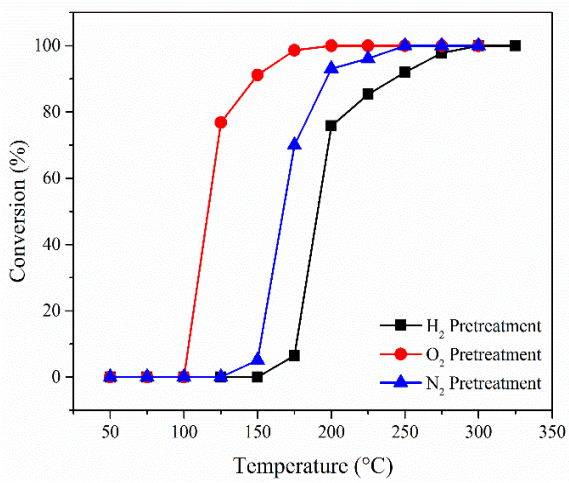

Fig.9. Effect of various pretreatment conditions on the activity of Co/CeO_2-SiO_2 specimen, reaction conditions: 2% CO, 20% O_2 and balanced with Ar, GHSV = 60,000 ml/g_{cat} h.

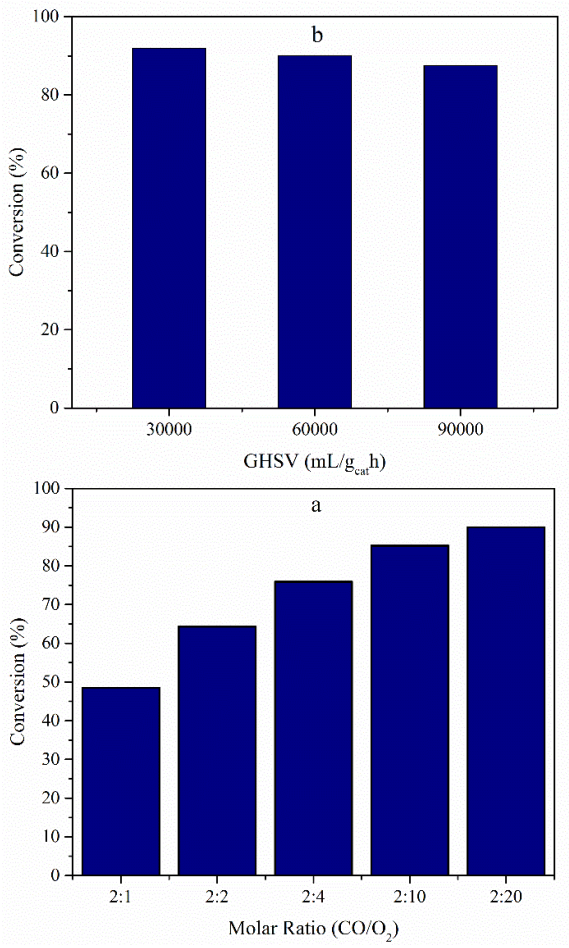

Fig. 10. Role of a) feed composition (GHSV = 60000 ml/g_{cat} h) and b) GHSV on CO conversion (at CO/O_2 = 2/20 molar ratio, $T_{reaction}$ = 150 °C

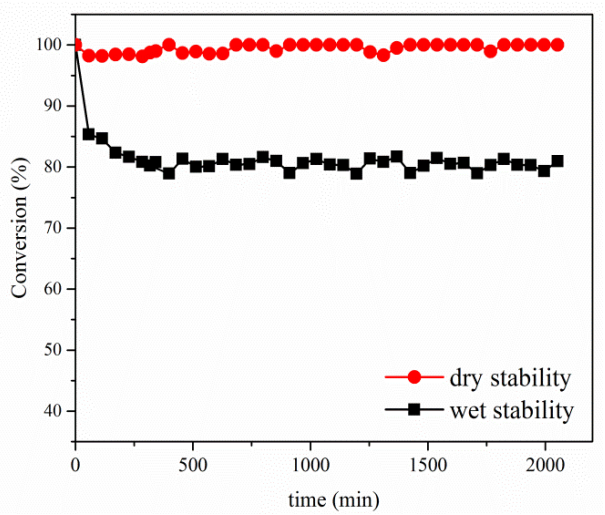

Fig. 11. Long-term lifetime examination of CO oxidation reaction over Co/CeO_2-SiO_2 specimen under dry feed (2% CO and 20% O_2) and wet feed (4% H_2O, 10% CO_2, 2% CO and 20% O_2), GHSV = 60000 ml/g_{cat} h, $T_{reaction}$ = 150 °C

4. Conclusion

Different compounds of silica structures composed of ceria were synthesized by different methods and used as supports for different active metals in the CO oxidation process. The results showed that the CuO/CeO_2-SiO_2 had excellent catalytic performance. High surface area, crystallinity, and reducibility may cause its higher activity. Also, the performance of various metal oxides as active phases on this support was evaluated, and it was found that cobalt oxide exhibited a very high performance owing to the generation of Co_3O_4 spinel species. The findings illustrated that introducing cobalt to the carrier structure significantly enhanced the catalyst's surface area more than the pure support and increased the catalyst activity.

Furthermore, an improvement in the catalytic activity was seen in the pretreated catalyst under an oxidative atmosphere. In addition, the influence of the change of GHSV and molar ratios on CO conversion was investigated, along with the performance of the optimum catalyst. During 36 hours of stream dry durability examination, no notable drop was perceived in the catalytic performance of this catalyst.

Acknowledgments

The authors gratefully appreciate the University of Kashan's financial support (Grant No. 158426/16).

Competing interests

The authors declare that they have no competing interests.

References

[1] E.-Y. Ko, E.D. Park, K.W. Seo, H.C. Lee, D. Lee, S. Kim, Selective CO oxidation in the presence of hydrogen over supported Pt catalysts promoted with transition metals, Korean J. Chem. Eng. 23 (2006) 182-187.
[2] J. Xu, Y.-Q. Deng, X.-M. Zhang, Y. Luo, W. Mao, X.-J. Yang, L. Ouyang, P. Tian, Y.-F. Han, Preparation, characterization, and kinetic study of a core–shell Mn3O4@SiO2 nanostructure catalyst for CO oxidation, ACS Catal. 4(11) (2014) 4106-4115.
[3] F. Yang, J. Huang, T. Odoom-Wubah, Y. Hong, M. Du, D. Sun, L. Jia, Q. Li, Efficient Ag/CeO2 catalysts for CO oxidation prepared with microwave-assisted biosynthesis, Chem. Eng. J. 269 (2015) 105-112.
[4] Z. Fu, L. Liu, Y. Song, Q. Ye, S. Cheng, T. Kang, H. Dai, Catalytic oxidation of carbon monoxide, toluene, and ethyl acetate over the xPd/OMS-2 catalysts: effect of Pd loading, Frontiers of Chem. Sci. Eng. 11 (2017) 185-196.
[5] J.-X. Liang, J. Lin, X.-F. Yang, A.-Q. Wang, B.-T. Qiao, J. Liu, T. Zhang, J. Li, Theoretical and experimental investigations on single-atom catalysis: Ir1/FeOx for CO oxidation, J. Phys. Chem. C 118(38) (2014) 21945-21951.
[6] Y. Shi, X. Hu, J. Zhao, X. Zhou, B. Zhu, S. Zhang, W. Huang, CO oxidation over Cu2O deposited on 2D continuous lamellar gC3N4, New J. Chem. 39(8) (2015) 6642-6648.
[7] D. Zhang, H. Zhang, Y. Yan, Catalytic activity of copper-ceria catalysts supported on different zeolites for CO oxidation, Korean J. Chem. Eng. 33 (2016) 1846-1854.
[8] S.A. Mock, S.E. Sharp, T.R. Stoner, M.J. Radetic, E.T. Zell, R. Wang, CeO2 nanorods-supported transition metal catalysts for CO oxidation, J. Colloid and Interface Sci. 466 (2016) 261-267.
[9] O. Aktas, S. Yasyerli, G. Dogu, T. Dogu, Effect of synthesis conditions on the structure and catalytic performance of V-and Ce-incorporated SBA-15-like materials in propane selective oxidation, Indust. Eng. Chem. Res. 49(15) (2010) 6790-6802.
[10] N. Pal, E.-B. Cho, D. Kim, C. Gunathilake, M. Jaroniec, Catalytic activity of CeIVO2/Ce2IIIO3-silica mesoporous composite materials for oxidation and esterification reactions, Chem. Eng. J. 262 (2015) 1116-1125.
[11] N. Pal, E.-B. Cho, D. Kim, Synthesis of ordered mesoporous silica/ceria–silica composites and their high catalytic performance for solvent-free oxidation of benzyl alcohol at room temperature, RSC Adv. 4(18) (2014) 9213-9222.
[12] N. Pal, E.B. Cho, A.K. Patra, D. Kim, Ceria-Containing Ordered Mesoporous Silica: Synthesis, Properties, and Applications, ChemCatChem 8(2) (2016) 285-303.
[13] O.G. Vargas, J. De Los Reyes Heredia, A.M. Castellanos, L. Chen, J. Wang, Cerium incorporating into MCM-41 mesoporous materials for CO oxidation, Mater. Chem. Phys. 139(1) (2013) 125-133.
[14] W. Zhu, K. Tang, J. Li, W. Liu, X. Niu, G. Zhao, X. Ma, Z. Liu, H. Wei, Y. Yang, The effect of copper species in copper-ceria catalysts: structure evolution and enhanced performance in CO oxidation, RSC Adv. 6(52) (2016) 46966-46971.
[15] J.-H. Park, J.H. Cho, S.E. Kang, K.H. Cho, T.W. Lee, H.S. Han, C.-H. Shin, Low-temperature CO oxidation over water tolerant Pt catalyst supported on Al-modified CeO2, Korean J. Chem. Eng. 30 (2013) 598-604.
[16] W. Robert, W. Heberton, S.B.D. Carlos, V.L. LR, E. Dario, Easy Access to Metallic Copper Nanoparticles with High Activity and Stability for CO Oxidation, ACS Appl. Mater. Interface. 7(15) (2015) 7987-94. 10.1021/acsami.5b00129.
[17] S. Royer, D. Duprez, Catalytic oxidation of carbon monoxide over transition metal oxides, ChemCatChem 3(1) (2011) 24-65.
[18] H.-K. Lin, H.-C. Chiu, H.-C. Tsai, S.-H. Chien, C.-B. Wang, Synthesis, characterization and catalytic oxidation of carbon monoxide over cobalt oxide, Catal. letter. 88 (2003) 169-174.
[19] F. Grillo, M.M. Natile, A. Glisenti, Low temperature oxidation of carbon monoxide: the influence of water and oxygen on the reactivity of a Co3O4 powder surface, Appl. Catal. B: Environ. 48(4) (2004) 267-274.
[20] K.A. Halim, M. Khedr, M. Nasr, A. El-Mansy, Factors affecting CO oxidation over nanosized Fe2O3, Mater. Res. Bullet. 42(4) (2007) 731-741.
[21] T. Cheng, Z. Fang, Q. Hu, K. Han, X. Yang, Y. Zhang, Low-temperature CO oxidation over CuO/Fe2O3 catalysts, Catal. Commun. 8(7) (2007) 1167-1171.
[22] H.A. Elazab, S. Moussa, K.W. Brinkley, B.F. Gupton, M.S. El-Shall, The continuous synthesis of Pd supported on Fe3O4 nanoparticles: A highly effective and magnetic catalyst for CO oxidation, Green Process. Synthesis 6(4) (2017) 413-424.
[23] K. Rida, A.L. Cámara, M. Peña, C. Bolívar-Díaz, A. Martínez-Arias, Bimetallic Co–Fe and Co–Cr oxide systems supported on CeO2: Characterization and CO oxidation catalytic behaviour, Int. J. Hydrogen Energy 40(34) (2015) 11267-11278.
[24] A. Biabani-Ravandi, M. Rezaei, Low temperature CO oxidation over Fe–Co mixed oxide nanocatalysts, Chem. Eng. J. 184 (2012) 141-146.
[25] D. Wu, R. Jia, M. Wen, S. Zhong, Q. Wu, Y. Fu, S. Yu, Ultrastable PtCo/Co3O4–SiO2 nanocomposite with active lattice oxygen for superior catalytic activity toward CO oxidation, Inorganic Chem. 59(2) (2019) 1218-1226.

[26] K. Tadanaga, K. Morita, K. Mori, M. Tatsumisago, Synthesis of monodispersed silica nanoparticles with high concentration by the Stöber process, J. Sol-Gel Sci. Technol. 68 (2013) 341-345.
[27] B. Bai, H. Arandiyan, J. Li, Comparison of the performance for oxidation of formaldehyde on nano-Co3O4, 2D-Co3O4, and 3D-Co3O4 catalysts, Appl. Catal. B: Environ. 142 (2013) 677-683.
[28] R. Locus, D. Verboekend, R. Zhong, K. Houthoofd, T. Jaumann, S. Oswald, L. Giebeler, G. Baron, B.F. Sels, Enhanced acidity and accessibility in Al-MCM-41 through aluminum activation, Chem. Mater. 28(21) (2016) 7731-7743.
[29] P.W. Dunne, A.M. Carnerup, A. Wegrzyn, S. Witkowski, R.I. Walton, Hierarchically structured ceria-silica: synthesis and thermal properties, J. Phys. Chem. C 116(24) (2012) 13435-13445.
[30] T. Campbell, M.A. Newton, V. Boyd, D.F. Lee, J. Evans, Effects of precursor and support variation in the genesis of uranium oxide catalysts for CO oxidation and selective reduction of NO: Synthesis and characterization, J. Phys. Chem. B 109(7) (2005) 2885-2893.
[31] S. Zeng, Y. Wang, S. Ding, J.J. Sattler, E. Borodina, L. Zhang, B.M. Weckhuysen, H. Su, Active sites over CuO/CeO2 and inverse CeO2/CuO catalysts for preferential CO oxidation, J. Power Source. 256 (2014) 301-311.
[32] M. Thommes, K. Kaneko, A.V. Neimark, J.P. Olivier, F. Rodriguez-Reinoso, J. Rouquerol, K.S. Sing, Physisorption of gases, with special reference to the evaluation of surface area and pore size distribution (IUPAC Technical Report), Pure and Appl. Chem. 87(9-10) (2015) 1051-1069.
[33] O. Aktas, S. Yasyerli, G. Dogu, T. Dogu, Structural variations of MCF and SBA-15-like mesoporous materials as a result of differences in synthesis solution pH, Mater. Chem. Phys.131(1-2) (2011) 151-159.
[34] W. Wang, P. Liu, M. Zhang, J. Hu, F. Xing, The pore structure of phosphoaluminate cement, Open J. Composite Mater. 2 (2012). 10.4236/ojcm.2012.23012.
[35] M. Thommes, Physical adsorption characterization of nanoporous materials, Chemie Ingenieur Technik 82(7) (2010) 1059-1073.
[36] N. Bayat, M. Rezaei, F. Meshkani, COx-free hydrogen and carbon nanofibers production by methane decomposition over nickel-alumina catalysts, Korean J. Chem. Eng. 33(2) (2016) 490-499.
[37] S. Mobini, F. Meshkani, M. Rezaei, Synthesis and characterization of nanocrystalline copper–chromium catalyst and its application in the oxidation of carbon monoxide, Process Safet. Environm. Protect. 107 (2017) 181-189.
[38] Y. Liu, D. Mao, J. Yu, X. Guo, Z. Ma, Low-temperature CO oxidation on CuO-CeO2 catalyst prepared by facile one-step solvothermal synthesis: Improved activity and moisture resistance via optimizing the activation temperature, Fuel 332 (2023) 126196.
[39] J. Xiaoyuan, L. Guanglie, Z. Renxian, M. Jianxin, C. Yu, Z. Xiaoming, Studies of pore structure, temperature-programmed reduction performance, and micro-structure of CuO/CeO2 catalysts, Appl. Surf. Sci. 173(3-4) (2001) 208-220.
[40] M. Tepluchin, M. Casapu, A. Boubnov, H. Lichtenberg, D. Wang, S. Kureti, J.D. Grunwaldt, Fe and Mn-Based Catalysts Supported on γ-Al2O3 for CO Oxidation under O2-Rich Conditions, ChemCatChem 6(6) (2014) 1763-1773.
[41] L. Zhang, L. Dong, W. Yu, L. Liu, Y. Deng, B. Liu, H. Wan, F. Gao, K. Sun, L. Dong, Effect of cobalt precursors on the dispersion, reduction, and CO oxidation of CoOx/γ-Al2O3 catalysts calcined in N2, J. Colloid and Interface Sci. 355(2) (2011) 464-471.
[42] S. Karimi, F. Meshkani, M. Rezaei, A. Rastegarpanah, Thermocatalytic decomposition of CH4 over Ni/SiO2.MgO catalysts prepared via surfactant-assisted urea precipitation method, Fuel 284 (2021) 118866.
[43] S. Mobini, F. Meshkani, M. Rezaei, Surfactant-assisted hydrothermal synthesis of CuCr2O4 spinel catalyst and its application in CO oxidation process, J. Environm. Chem. Eng. 5(5) (2017) 4906-4916.
[44] S. Karimi, F. Meshkani, M. Rezaei, A. Rastegarpanah, The influence of promoters on the catalytic behavior of the Ni/SiO2.MgO catalysts for thermocatalytic decomposition of methane reaction, Fuel 372 (2024) 131945.
[45] K.M. Cook, Understanding Noble Metal Addition in Cobalt Fischer Tropsch Catalysts, Brigham Young University (2012).
[46] A. Biabani-Ravandi, M. Rezaei, Z. Fattah, Catalytic performance of Ag/Fe2O3 for the low temperature oxidation of carbon monoxide, Chem. Eng. J. 219 (2013) 124-130.
[47] D. Gu, C.-J. Jia, C. Weidenthaler, H.-J. Bongard, B. Spliethoff, W. Schmidt, F. Schüth, Highly ordered mesoporous cobalt-containing oxides: structure, catalytic properties, and active sites in oxidation of carbon monoxide, J. American Chemical Soci. 137(35) (2015) 11407-11418.
[48] X. Xi, S. Ma, J.-F. Chen, Y. Zhang, Promotional effects of Ce, Mn and Fe oxides on CuO/SiO2 catalysts for CO oxidation, J. Environm. Chem. Eng. 2(2) (2014) 1011-1017.
[49] P.M. Kouotou, H. Vieker, Z. Tian, P.T. Ngamou, A. El Kasmi, A. Beyer, A. Gölzhäuser, K. Kohse-Höinghaus, Structure–activity relation of spinel-type Co–Fe oxides for low-temperature CO oxidation, Catal. Sci. Technol. 4(9) (2014) 3359-3367.